Sub-Grid Model Improving Shrinking Core Simulations of Redox-Sensitive Technetium Release From Slag Cement Waste Forms – 17295

Gregory P. Flach
Savannah River National Laboratory

ABSTRACT

Numerical simulation of Tc transport in reducing cementitious materials undergoing oxidation is challenging because the effective solid-solute partition coefficient (K_d) varies greatly between the reduced and oxidized states, assuming the Tc mass loading far exceeds that required to reach solubility in the aqueous phase, as is typical in waste disposal. In a conventional finite-volume formulation, the local aqueous concentration increases orders of magnitude when a computational cell switches from a reducing to oxidizing condition, which is an artifact of numerical discretization. In principal such artifacts can be reduced to an insignificant level by refining the computational grid. However, this approach is not feasible in typical facility scale applications due to computer runtime and storage limitations. In this paper an alternative sub-grid Tc release model is derived to approximately capture redox processes occurring at scales smaller than the computational mesh. This alternative approach introduces minimal additional computational expense, while significantly reducing numerical artifacts in the form of Tc concentration / flux spikes. The method is illustrated for two simple geometries and the Savannah River Site Saltstone waste Disposal Facility. The sub-grid model is shown to significantly reduce artificial spikes in Tc-99 release, resulting in more physically realistic numerical simulations.

INTRODUCTION

Ground blast furnace slag is commonly incorporated in cementitious waste forms and barriers to improve physical properties and/or create reducing conditions. The latter condition is particularly favorable for retaining Tc-99, which is mobile in its oxidized (+7) state and largely precipitated and immobile under reducing conditions (+4 state). Depending on the waste loading, the pore fluid concentration of Tc-99 under oxidized conditions can be orders of magnitude higher than the solubility limit under reducing conditions, around 1.E-8 mol/L. This orders of magnitude disparity creates a significant numerical modeling challenge as slag cement oxidizes over time due to infiltrating dissolved oxygen. If a computational cell switches abruptly (e.g., over a time step) from the reduced to oxidized state, then the local aqueous concentration will spike orders of magnitude, assuming the typical case of significant Tc mass originally held-up in the solid phase. In principal, numerical artifacts of this nature can be reduced to an arbitrarily low level through refinement of the computational grid. However, practical constraints on grid size for a facility-scale simulation often preclude this approach.

An alternative approach is to introduce a sub-grid scale model to the standard finite volume numerical technique. The novel sub-grid model described herein is based on the concept that, in a computational cell undergoing oxidation, dissolved oxygen ingress and Tc-99 release occur at relatively constant rates because both species

experience the same advective flow field and similar diffusion processes. The concept results in a derived partition coefficient (K_d) that varies through time as a function of the reduction capacity remaining in the solid phase, and reflects the combined effects of solubility control and sub-grid scale oxidation. The sub-grid modeling approach achieves computational efficiency by avoiding mesh refinement at the minimal expense of an algebraic grid cell calculation between successive time steps.

The remainder of the paper describes development of the sub-grid model and presents numerical simulation results for an illustrative, simple, shrinking-core geometry and the Savannah River Site (SRS) Saltstone Disposal Facility. The sub-grid model is shown to significantly reduce artificial spikes in Tc-99 release, resulting in more physically realistic numerical simulations.

METHOD DEVELOPMENT

Tc transport properties for cementitious materials recommended by Kaplan and Li (2013) [1] are summarized in Table I. The typical evolution of chemical states is Reduced / Young → Reduced / Moderate → Oxidized / Moderate → Oxidized / Aged. The pH transition from Young to Moderate age occurs relatively quickly in the context of long Performance Assessment timeframes, and the Moderate to Aged transition involves a relatively minor change in sorption coefficient. Thus the principal chemical change of interest is the Reduced to Oxidized transition. To simplify numerical implementation going forward, only an Eh transition from solubility control at 1.0E-8 mol/L to sorption control with K_d = 0.5 mL/g is considered, the latter conservatively chosen as the minimum of the Moderate and Aged values.

TABLE I. Tc transport parameters for cementitious materials.

Cementitious Material	**Young Cement 1st Stage (pH ~12)**	**Moderately-aged Cement 2nd Stage (pH ~10.5)**	**Aged Cement 3rd Stage (pH ~5.5)**
Reduced	6 x 10^{-7} mol/L solubility	1 x 10^{-8} mol/L solubility	0.5 mL/g sorption (K_d)
Oxidized	0.8 mL/g sorption (K_d)	0.8 mL/g sorption (K_d)	0.5 mL/g sorption (K_d)

Following Kaplan and Hang (2003) [2], a PORFLOW code (http://www.acricfd.com/software/porflow) shrinking-core simulation of slag oxidation via dissolved oxygen ingress is used to define the Eh condition of the cementitious material throughout space and time. Slag reduction (reaction) capacity is defined by an initial solid-phase concentration ($c_{Slag,0}$) expressed in units of milliequivalents per gram (meq e-/g). Dissolved oxygen at its solubility limit (c_{Ox}), introduced through boundaries and internal sources, migrates through advection and/or diffusion into the cementitious material and consumes the slag reaction capacity. Values representative of the SRS Saltstone Disposal Facility are $c_{Slag,0}$ = 0.607 meq e-/g for saltstone grout, $c_{Slag,0}$ = 0.178 meq e-/g for slag concrete, and c_{Ox} = 1.06E-03 meq e-/mL [3]. In model simulations the oxidation

fraction, ranging from 0 to 1, is tracked through time for each computational cell. With respect to Tc transport, PORFLOW version 6.30.2 does not provide a built-in means for implementing both solubility control under reducing conditions, and a transition from solubility to sorption control as a function of oxidation fraction. However, both phenomena can be implemented through a user-defined effective partition coefficient (K_d) function that varies from cell to cell through time.

Figure 1 illustrates the concept behind the sub-grid model used to define the time-varying K_d in each computational cell. The upper image represents steady, one-dimensional, advection-dominated, flow through a cementitious material that is initially reduced with full reduction capacity present (blue shading). Oxidation (red shading) occurs at a constant rate, due to dissolved oxygen ingress through steady advection from the left boundary. Oxidation is assumed to occur along a sharp front, separating distinct fully-oxidized and fully-reduced (unimpacted) sub-regions of the domain. The solid boxes indicate computational grid cells for numerical simulation. At the illustrated snapshot in time (③), the oxidation front has advanced midway through the center computational cell. Because the oxidation front is sharp, both oxidized and reduced sub-regions exist within the active computational cell.

Under this concept, Tc is released from the solid to the liquid phase uniformly over the period the constant-rate oxidation front enters the cell until it leaves. The lower portion of Figure 1 illustrates the corresponding K_d variation. While Tc is under solubility control, the effective K_d value is large. The moment the oxidation front first enters the computational cell, K_d makes a step change to a lower value. K_d then gradually decreases further as the oxidation front advances through the cell.

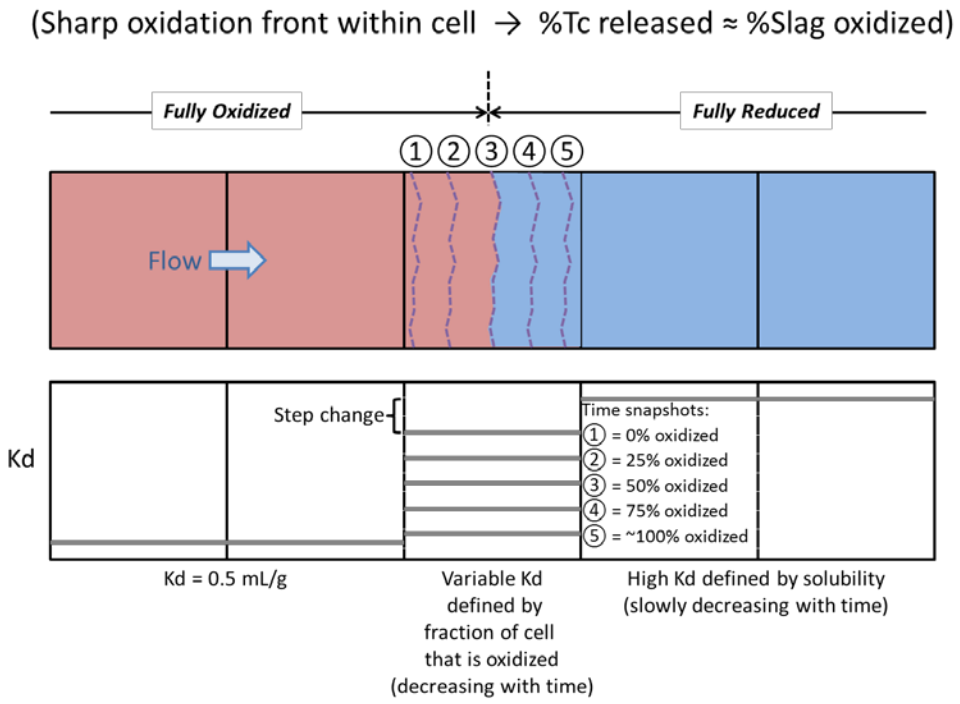

Fig. 1. Concept behind sub-grid model for Tc release.

Advective transport

To derive a K_d function that implements this general concept, a simple advection-only (or advection-dominated) transport scenario is considered first, as depicted in Figure 2, scenario ①. Here oxygen enters the cell through advection and Tc leaves the cell subject to the same Darcy velocity, U. The mass flowrate of Tc leaving the cell is

$$F = \frac{V}{\Delta z} c_L U \qquad \text{(Eq. 1)}$$

where V = total volume, Δz = cell length, and c_L = Tc liquid-phase concentration. Similarly, the mass flowrate of oxygen entering the cell is

$$G = \frac{V}{\Delta z} c_{Ox} U \qquad \text{(Eq. 2)}$$

where again c_{Ox} = dissolved concentration of oxygen at solubility.

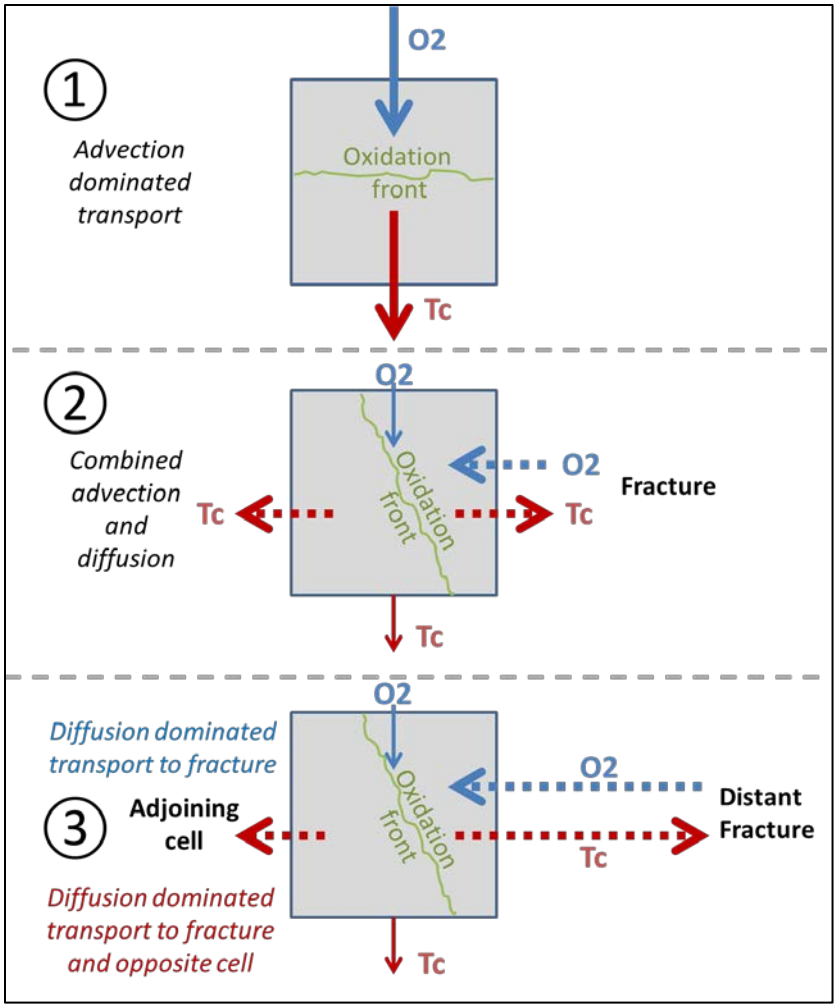

Fig. 2. Oxidation and transport scenarios for oxygen and Tc.

An oxidation front moving through a cell effectively functions as a moving line source. That is, oxidation at constant rate acts approximately as a constant source of Tc to the aqueous phase. Assuming that advection is sufficiently fast to sweep Tc from the cell and prevent an accumulation, then the mass rate of Tc leaving the cell should approximately match the constant source term. For a constant flow rate, this implies a constant liquid phase concentration, c_L. Under this assumption the depletion time for Tc is

$$\Delta t_F = \frac{m_{Tc,0}}{F} = \frac{m_{Tc,0}}{V c_L U/\Delta z} \quad \text{(Eq. 3)}$$

Similarly, the concentration of dissolved oxygen is constant and the depletion time for slag reaction capacity is

$$\Delta t_G = \frac{m_{slag,0}}{G} = \frac{\rho_b V c_{slag,0}}{V c_{Ox} U/\Delta z} \quad \text{(Eq. 4)}$$

Under these advective transport conditions, the speed of the oxidation front is $c_{Ox}U/c_{Slag,0}\rho_b$ compared to a pore velocity of U/Sn. For saltstone, S = 1 mL liquid /

mL void, n = 0.58 mL void / mL, c_{Ox} = 1.06e-3 meq e-/mL liquid, $c_{Slag,0}$ = 0.607 meq e-/g solid, and ρ_b = 1.01 g solid/mL [3], and the ratio of the oxidation and advective transport speeds is

$$\frac{c_{Ox}U/c_{Slag,0}\rho_b}{U/Sn} = \frac{c_{Ox}Sn}{c_{Slag,0}\rho_b} = 0.001 \quad \text{(Eq. 5)}$$

That is, the oxidation front advances at a rate three orders of magnitude slower than advection of an unretarded solute. Any Tc released to the liquid will therefore be advected out of the cell in short order compared to the rate of cell oxidation. Thus, Tc should be depleted at approximately the same time as slag reaction capacity. Equating Equations (3) and (4) and solving for c_L produces

$$c_L = \frac{c_{T,0}c_{Ox}}{\rho_b c_{slag,0}} \quad \text{(Eq. 6)}$$

for the constant Tc concentration needed to achieve an constant Tc flux. The corresponding effective Tc partition coefficient function can then be derived as

$$K_d \equiv \frac{c_s}{c_L} = \frac{m_s/\rho_b V}{c_L} = \frac{m-m_L}{\rho_b V c_L} = \frac{m-SnVc_L}{\rho_b V c_L} = \frac{m/V}{\rho_b c_L} - \frac{Sn}{\rho_b} = \frac{c_T}{\rho_b c_L} - \frac{Sn}{\rho_b} = \frac{c_{T,0}}{\rho_b c_L}\cdot\frac{c_T}{c_{T,0}} - \frac{Sn}{\rho_b} \quad \text{(Eq. 7)}$$

The prior assumption that Tc and slag are depleted at the same rate implies

$$\frac{c_T}{c_{T,0}} = x_{Re} = (1 - x_{Ox}) = 1 - \frac{c_{slag}}{c_{slag,0}} \quad \text{(Eq. 8)}$$

Equation (6) can also be rearranged as

$$\frac{c_{T,0}}{\rho_b c_L} = \frac{c_{slag,0}}{c_{Ox}} \quad \text{(Eq. 9)}$$

Substituting Equations (8) and (9) into Equation (7) yields the desired K_d functionality for the "redox" transition, $x_{Re} \to 0$:

$$K_d{}^{redox} = \frac{c_{slag,0}}{c_{Ox}}x_{Re} - \frac{Sn}{\rho_b} \quad \text{(Eq. 10)}$$

Note that this effective partition coefficient is a function of only one time-varying quantity, $x_{Re} = 1 - x_{Ox}$. To avoid negative values of K_d and implement fully oxidized conditons ($x_{Re} = 0$), Equation (10) is modified to

$$K_d{}^{redox} = max\left[\frac{c_{slag,0}}{c_{Ox}}x_{Re} - \frac{Sn}{\rho_b}, K_{d,Ox}\right] \quad \text{(Eq. 11)}$$

The K_d functionality needed to implement solubility control ($x_{Re} = 1$) was derived by Jordan and Flach (2013, Eq. 2.16) [4] as

$$K_d{}^{solubility} = max\left[\frac{c_T - nSC_{sol}}{\rho_b C_{sol}}, K_{d,Re}\right] \quad \text{(Eq. 12)}$$

The full range of conditions ($0 \leq x_{Re} \leq 1$) can be approximated by blending Equations (11) and (12) with an x_{Re} weighting function

$$K_d = {x_{Re}}^p {K_d}^{solubility} + (1 - {x_{Re}}^p){K_d}^{redox} \quad \text{(Eq. 13)}$$

A rapid transition from ${K_d}^{solubility}$ to ${K_d}^{redox}$ when a cell starts becoming oxidized requires $p \gg 1$. The somewhat arbitrary value $p = 200$ was deemed satisfactory based on empirical testing [5].

Figure 3 shows a stack of 10 computational cells containing slag and Tc, plus inlet and outlet cells. Figure 4 illustrates Tc flux results for this computational system based on two Tc release models. The left image illustrates outlet flux when Tc K_d transitions relatively abruptly from a high, solubility-control, value (Equation (12), while reduction capacity is present) to K_d = 0.5 mL/g as $x_{Re} \to 0$ [4]. Because Tc released from upgradient cells is recaptured by solubility control in downstream cells, Tc mass builds up just ahead of the oxidation front and is only released at the outlet in significant amounts when the last cell becomes oxidized. The right image illustrates the sub-grid model derived herein and summarized by Equation (13). Here Tc is released gradually as the oxidation front advances through the last interior grid cell. In these advection-dominated transport simulations the sub-grid model is observed to produce much smoother Tc flux results.

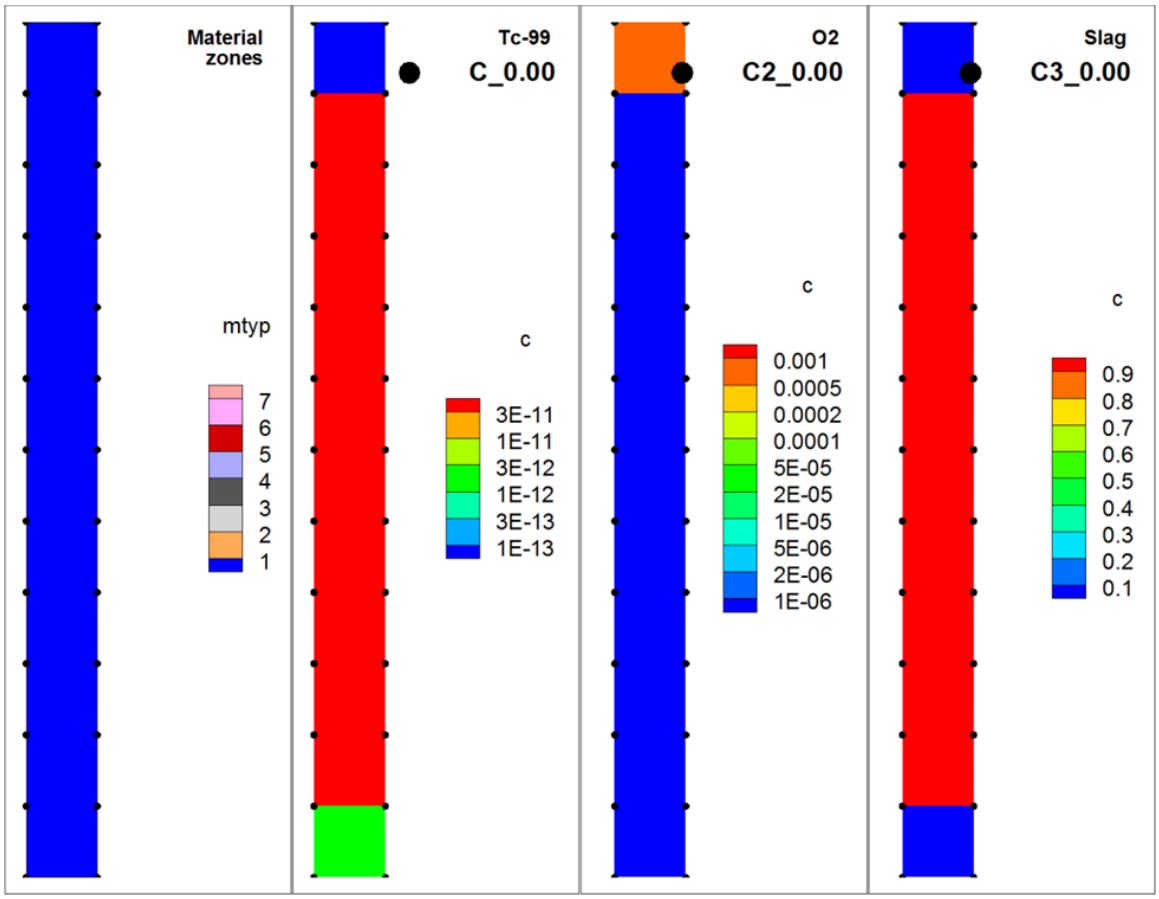

Fig. 3. Stack of 10 slag and Tc bearing grid cells; condition at time zero.

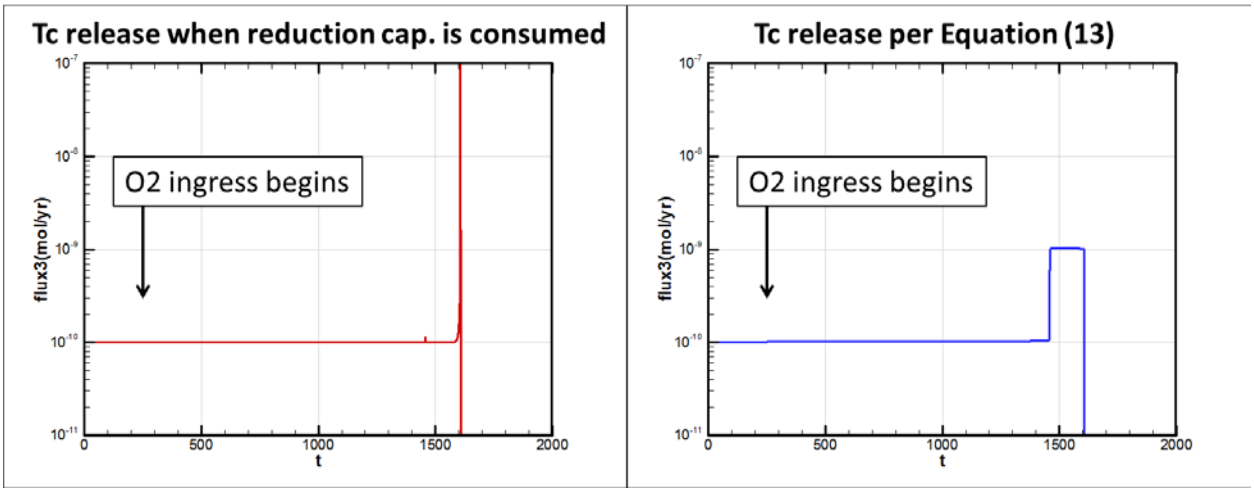

Fig. 4. Slag oxidation and Tc transport simulation for a stack of cells.

Advective-diffusive transport

The preceding analysis and numerical simulations involve only advective transport of dissolved oxygen and Tc. The Saltstone Disposal Facility Performance Assessment (PA) involves low permeability cementitious materials (grout, concrete) for which diffusion is often the dominant transport mode over portions of the simulation period. At other times, advection and diffusion may have similar importance and/or advection may dominate. Thus, extension of Equation (13) to the more general case of advective-diffusive transport is desirable.

For context consider Figure 5, which depicts a hypothetical column composed of a discrete fracture passing through saltstone grout encapsulated in a concrete barrier. Soil occupies regions outside the engineered structure. Transport is advection-dominated within the fracture but may vary from advection to diffusion-dominated in the surrounding matrix.

For the grout zone within the discrete fracture geometry, the nature of oxygen and Tc transport is similar to scenario ② depicted in Figure 2. Oxygen enters the top through advection and the fracture side by diffusion. Tc leaves the bottom by advection and *both* sides by lateral diffusion. Assuming for the moment that the diffusion distance is one cell width, Δx, the Tc and oxygen mass flowrate equations analogous to Equations (1) and (2) are

$$F = \frac{V}{\Delta z} c_L U + 2 \frac{V}{\Delta x} D_e \frac{c_L}{\Delta x} \quad \text{(Eq. 14)}$$

$$G = \frac{V}{\Delta z} c_{Ox} U + \frac{V}{\Delta x} D_e \frac{c_{Ox}}{\Delta x} \quad \text{(Eq. 15)}$$

where D_e is the effective diffusion coefficient of the porous medium. Note that Equation (14) contains a factor of two in the diffusion term, reflecting transport from both sides, whereas oxygen is available only from the fracture side. Following the same derivation process as before, the result is

$$K_d{}^{redox} = f_{Pe} \frac{c_{slag,0}}{c_{Ox}} x_{Re} - \frac{Sn}{\rho_b} \quad \text{(Eq. 16)}$$

where

$$f_{Pe} = 1 + \frac{1}{1 + Pe(\Delta x / \Delta z)^2} \quad \text{(Eq. 17)}$$

and Pe is the Peclet number

$$Pe = \frac{U \Delta z}{D_e} \quad \text{(Eq. 18)}$$

For advection-dominated transport, the Peclet number approaches infinity and $f_{Pe} \rightarrow 1$. Thus Equation (10) is recovered as a special case of Equation (16). For diffusion-dominated transport, Pe = 0 and f_{Pe} = 2, which effectively doubles the $K_d{}^{redox}$ value (the term Sn/ρ_b is small). Thus the range of f_{Pe} for scenario ② in Figure 2 is

effectively $1 \leq f_{Pe} \leq 2$.

Figure 6 shows Tc flux leaving the cementitious material / fracture zone for simulations (a) without a Tc sub-grid model (upper left), (b) assuming advection-dominated transport, Equation (10) or Equation (16) with f_{Pe}= 1 (upper right), and (c) assuming diffusion-dominated transport, Equation (16) with f_{Pe}= 2 (lower left). Without a sub-grid model for Tc release, the outlet flux exhibits a series of distinct spikes with magnitudes up to two orders of magnitude above the baseline (upper left). The sub-grid model assuming advective transport produces a smoother response with the oscillations ranging over about one order of magnitude (upper right). Further improvement is observed for the sub-grid model with f_{Pe}= 2. However, the oscillations are still significant, ranging over roughly half an order of magnitude (lower left).

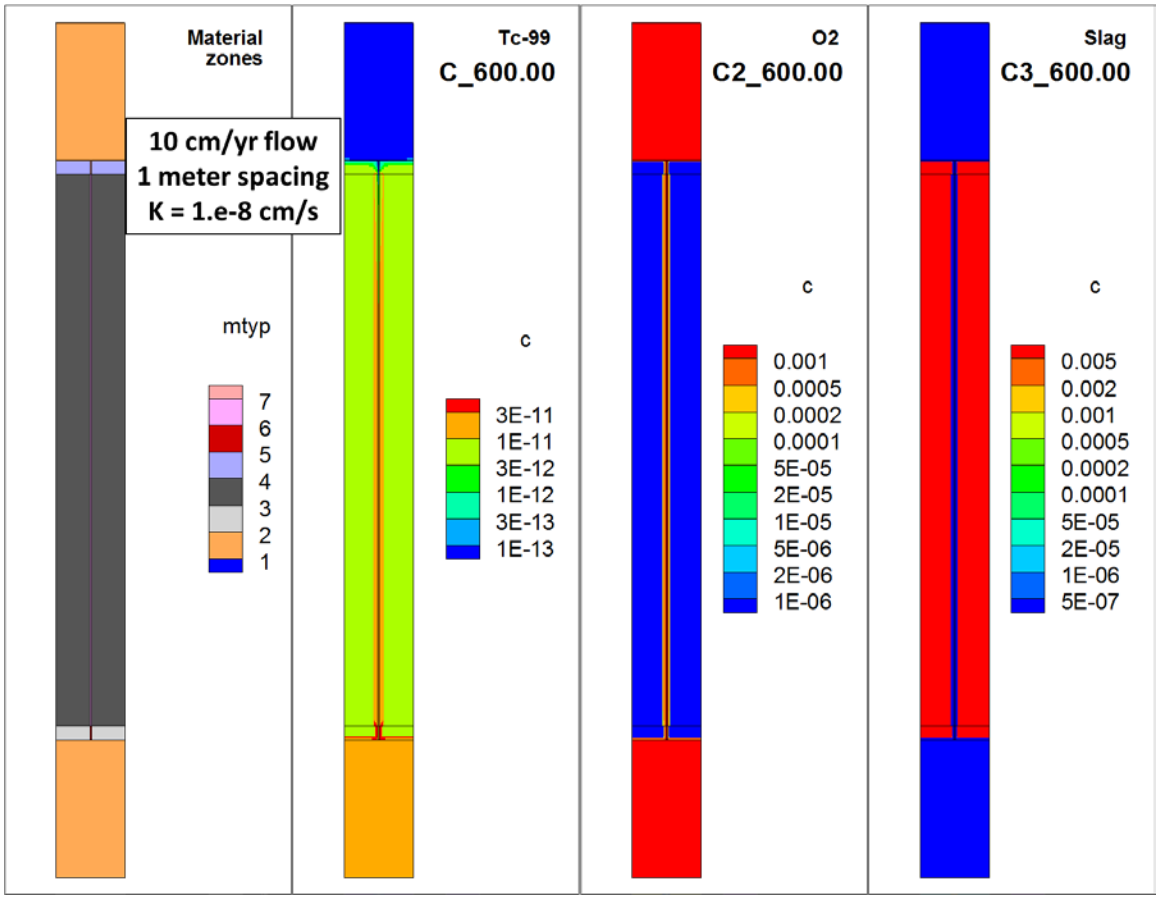

Fig. 5. Simulation of a discrete fracture; representative snapshot at t=600 yrs.

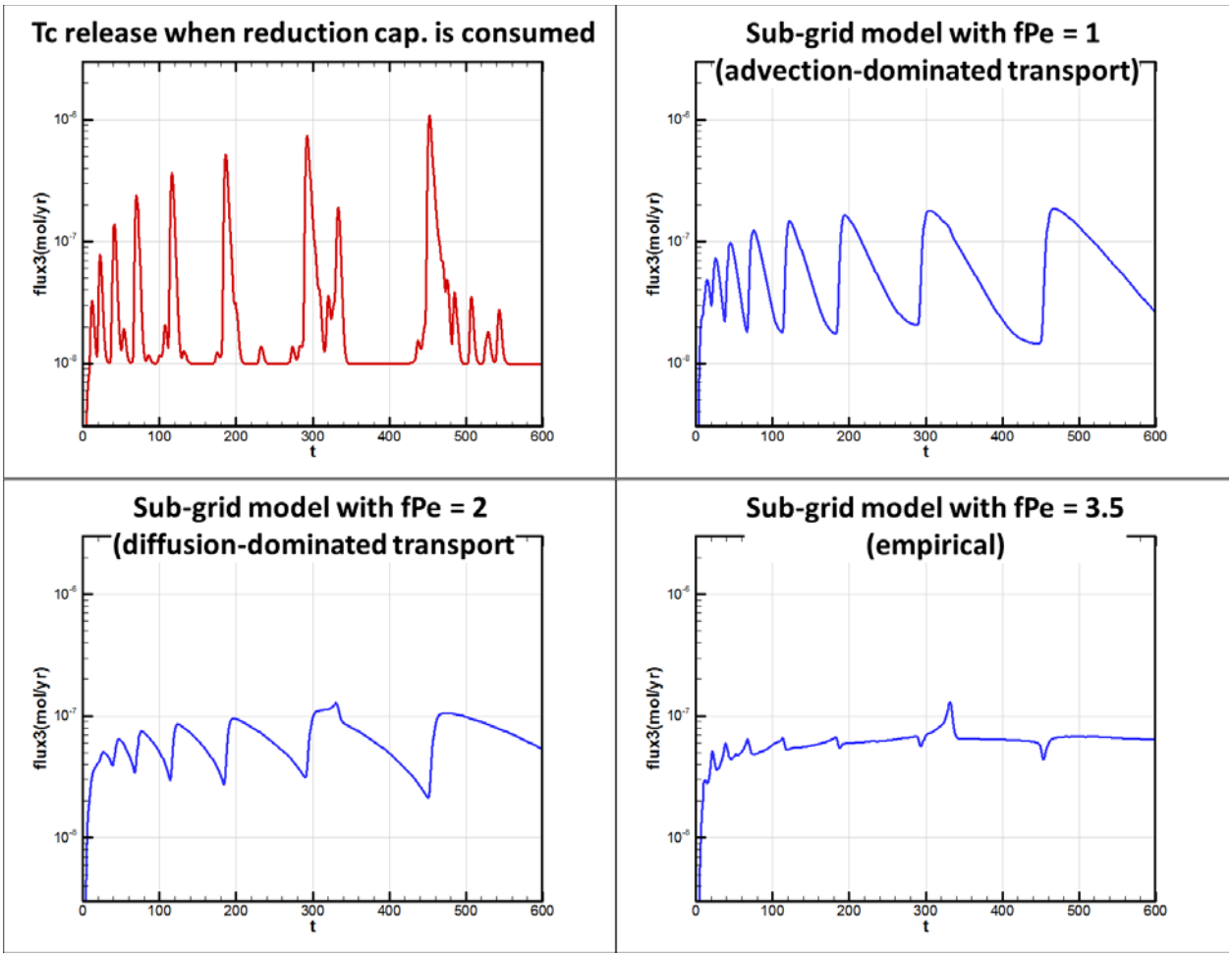

Fig. 6. Slag oxidation and Tc transport simulation for a discrete fracture.

Model refinement

Scenario ③ in Figure 2 likely explains the remaining discrepancy between model simulations and physical expectations. Once the oxidation front has penetrated the matrix, the diffusion distance for oxygen and Tc from and to the fracture, respectively, has lengthened considerably beyond Δx. However, the adjoining cell on the opposite side is still reduced and maintains a low concentration sink for Tc at a short distance. Therefore, the diffusive ingress of oxygen is much slower than the diffusive egress of Tc for scenario ③ compared to scenario ②. This observation implies that an even larger value of f_{Pe} is needed for scenario ③. An empirical investigation indicated an optimal value of approximately f_{Pe} = 3.5 for the geometry and timescale of the simulation illustrated in Figures 5 and 6. Figure 6 (lower right) illustrates the outlet flux results for this setting. The simulated Tc flux exhibits much smaller perturbations than the previous cases, and approaches the smooth variation expected from physical considerations.

APPLICATION TO SALTSTONE FACILITY

Other scenarios of increasing sophistication beyond those shown in Figure 2 could be considered, resulting in additional K_d functions. One possibility would be to monitor evolving transport conditions on a cell-by-cell basis and compute K_d on the fly using functions selected from a palette of options. However, considering the myriad of different K_d variations that might result from different transport scenarios, a focus on saltstone system modeling is helpful toward narrowing the possibilities. Except for relatively early periods (several hundred to a few thousand years), cementitious materials and the facility cover system are significantly degraded in typical Saltstone Disposal Facility PA scenarios. The result tends to be advection-dominated flow. Therefore, Equation (10), or equivalently Equation (16) with f_{Pe}= 1, was selected for PA simulations.

Figure 7 illustrates simulated Tc release for the Saltstone Disposal Unit 2 design, for a hypothetical scenario in which the monolith is fractured [5]. Gas-phase oxygen in apertures is assumed to create local sources of dissolved oxygen distributed throughout the grout. Without a Tc subgrid model the simulated flux is erratic, reflecting abrupt Tc releases from discrete computational cells as they become oxidized over time. Spikes in Tc flux exceed two orders of magnitude. With implementation of the Tc sub-grid model the simulated Tc flux is remarkably smoother.

Figure 8 illustrates simulation results for Saltstone Disposal Unit 2 when the grout monolith is intact but slowly degrades, resulting in a gradual increase in permeability [5]. In this simulation early releases are constrained to a low level by Tc solubility and increase slowly due to increasing moisture flow. After about 30,000 years much larger releases are observed when the downward moving oxidation front reaches the disposal unit floor. Similar to Figure 8, the Tc release sub-grid model produces a marked reduction in flux spikes that are an artifact of the numerical grid resolution.

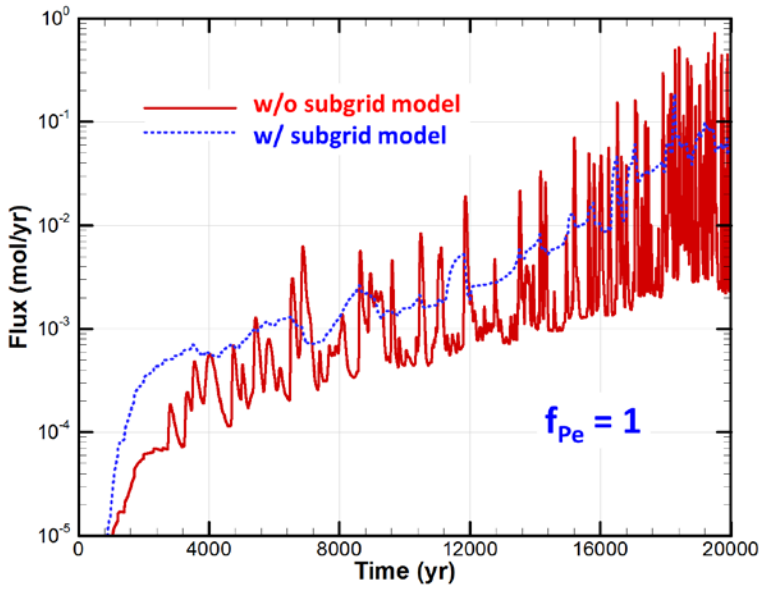

Fig. 7. Tc flux from Saltstone Disposal Unit 2 assuming hypothetical fractures in the monolith acting as oxygen sources.

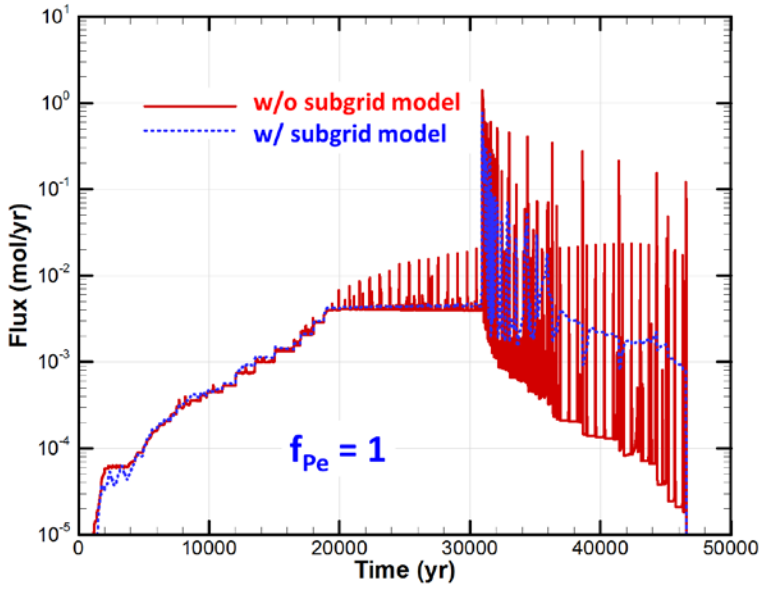

Fig. 8. Tc flux from Saltstone Disposal Unit 2 assuming an intact monolith.

CONCLUSION

Numerical simulation of Tc transport in reducing cementitious materials undergoing oxidation is challenging because the effective solid-solute partition coefficient (K_d) varies greatly between the reduced and oxidized states, assuming the Tc mass loading far exceeds that required to reach solubility in the aqueous phase, as is typical in waste disposal. In a conventional finite-volume formulation, the local aqueous concentration increases orders of magnitude when a computational cell switches from a reducing to oxidizing condition, which is an artifact of numerical discretization. In principal such artifacts can be reduced to an insignificant level by refining the computational grid. However, this approach is not feasible in typical facility scale applications due to computer runtime and storage limitations. In this paper an alternative sub-grid Tc release model was derived to approximately capture redox processes occurring at scales smaller than the computational mesh. This alternative approach introduces minimal additional computational expense, while significantly reducing numerical artifacts in the form of Tc concentration / flux spikes. The resulting numerical simulations are more physically realistic.

REFERENCES

1. D. I. KAPLAN and D. LI, “Solubility of Technetium Dioxides (TcO_2-c, $TcO_2 \cdot 1.6H_2O$ and $TcO_2 \cdot 2H_2O$) in Reducing Cementitious Material Leachates: A Thermodynamic Calculation,” Savannah River National Laboratory technical report SRNL-STI-2012-00769, Rev. 1 (2013).
2. D. I. KAPLAN and T. HANG, “Estimated duration of the subsurface reducing environment produced by the Z-Area Saltstone Disposal Facility (U),” Savannah River National Laboratory technical report WSRC-RP-2003-00362, Rev. 2 (2003).
3. SAVANNAH RIVER REMEDIATION LLC, “FY2014 Special Analysis for the Saltstone Disposal Facility at the Savannah River Site,” technical report SRR-CWDA-2014-00006, Rev. 2 (2014).
4. J. M. JORDAN and G. P. FLACH, “PORFLOW Modeling Supporting the FY13 Saltstone Special Analysis,” Savannah River National Laboratory technical report SRNL-STI-2013-00280, Rev. 0 (2013).
5. G. P. FLACH and G. A. TAYLOR, “PORFLOW Modeling Supporting the FY14 Saltstone Special Analysis,” Savannah River National Laboratory technical report SRNL-STI-2014-00083, Rev. 1 (2014).

ACKNOWLEDGEMENTS

This manuscript has been authored by Savannah River Nuclear Solutions, LLC under Contract No. DE-AC09-08SR22470 with the U. S. Department of Energy. The United States Government retains and the publisher, by accepting this article for publication, acknowledges that the United States Government retains a non-exclusive, paid-up, irrevocable, worldwide license to publish or reproduce the published form of this work, or allow others to do so, for United States Government purposes.